JOURNAL OF MATERIALS SCIENCE 17 (1982) 2831–2840

An explanation for the rate-of-loading and the duration-of-load effects in wood in terms of fracture mechanics

J. S. NADEAU, R. BENNETT
Department of Metallurgical Engineering, University of British Columbia, Vancouver, B.C., Canada

E. R. FULLER JR
National Bureau of Standards, Washington, D.C., USA

Wood is one of the few engineering materials for which design codes specify that the applied stress be contingent on the duration of the load. This is in recognition of the fact that the strength of wood appears to degrade with time when under stress. This paper describes a set of experiments in which the kinetics of wood fracture are examined. It is shown that the present results and those of earlier workers can be fully explained by a relatively simple model and mathematical analysis, based on fracture mechanics. According to these results, the delayed failure of wood is caused by subcritical crack growth. The model helps to reveal what must be done to incorporate the duration-of-load effect into timber design in a probabalistic manner.

1. Introduction

The fracture strength of many engineering materials depends upon how rapidly the stress is applied. This is particularly true of brittle materials like glass and some plastics. It is also true of wood.

Explanations for the phenomenon fall into two categories, those based on fracture mechanics [1, 2] and those invoking a structural damage mechanism [3, 4]. Since fracture mechanics makes no assumptions about mechanisms except to say that failure is by the extension of cracks, the two categories of explanations are not necessarily incompatible. This paper presents an explanation for the rate-of-loading effect in Douglas Fir Wood, based on the kinetics of subcritical crack growth. A subcritical crack is one that is too small to cause failure at the current stress. If, however, it is able to grow in response to the stress, the kinetics of its growth will dictate the endurance of the cracked component. Furthermore, it is sufficient, for purposes of failure prediction, to know only the kinetics of crack growth; the mechanism need not be understood.

The rate-of-loading effect is important primarily because it is an easily measured surrogate for delayed failure which is known in the wood literature as the duration-of-load effect. This effect is of great engineering importance, because it sets a limit on the allowable stresses in structures, based on the expected time under load. Thus, a timber structure that is expected to bear its loads for 10 years is allowed to have only 93% of the stress permitted in a structure designed for a life of 1 year [5].

Although there is ample evidence that a rate-of-loading effect exists in small clear wood specimens, Spencer [6] has recently shown that the effect seems to disappear in the weaker members of a set of dimension-lumber specimens. At the 95th percentile of breaking strength in Spencer's tests, the strength was about 40% higher for very fast loading rates than it was for very slow rates. However, at the 5th percentile, the strength appears to be independent of the loading rate. Since the strength at the 5th percentile is used as a design criterion in building codes, it would appear that

0022–2461/82/102831–10$03.70/0

the rate-of-loading effect and its counterpart, the duration-of-load effect, should not be used for dimension lumber. However, this paper is addressed primarily to the understanding of the phenomena that give rise to the rate-of-loading effect, rather than to the question of proper design strategies.

In two previous papers [1, 2] it was shown that, for cracks running *parallel to the grain* in Douglas Fir, the rate-of-loading effect could be explained in terms of subcritical crack growth. This involved the independent measurement of crack velocity, V, versus crack driving force, K, and the rate-of-loading effect. An analysis of the rate-of-loading effect based on fracture mechanics yielded a value for the slope of the V–K plot (65), which was in close agreement with the slope that was experimentally measured (62). However, timber structural members are not normally loaded in tension perpendicular to the grain and the present experiments extend the earlier results to the practical case of tension parallel to the grain.

The fracture mechanics approach to the rate-of-loading effect in brittle materials has been developed by Evans [7] and by Ritter and Sherburne [8, 9]. It is based upon the Griffith–Irwin equation describing strength, S, in terms of crack size, a, and an intrinsic material property called fracture toughness, K_c. It also utilizes an empirical relationship that describes crack kinetics:

$$S = K_c/Y\sqrt{a} \tag{1}$$

$$\frac{da}{dt} = V = AK_I^N \tag{2}$$

where Y, A and N are constants. In effect, failure by subcritical crack growth involves the gradual extension of a crack in accordance with Equation 2 until it reaches a critical value defined by Equation 1.

Using a more general form of Equation 1, i.e.

$$K = Y\sigma\sqrt{a} \tag{3}$$

where σ is simply the applied stress and K is the applied stress intensity ($K < K_c$), and combining Equation 3 with Equation 2 gives

$$\frac{da}{dt} = AY^N\sigma^N a^{N/2}. \tag{4}$$

Substituting the identity:

$$d\sigma/\dot{\sigma} = dt \tag{5}$$

leads to the integration

$$\int_{a_i}^{a_f} a^{-N/2}\,da = (AY^N/\dot{\sigma})\int \sigma^N d\sigma \tag{6}$$

and

$$\frac{2}{(N-2)}\left[a_i^{-(N-2/2)} - a_f^{-(N-2/2)}\right] = \frac{AY^N}{(N+1)}\sigma_f^{N+1} \tag{7}$$

where the subscripts i and f are used to indicate the initial condition before testing, and the final condition on fracture. It is usually more convenient to work with the strength than the crack length and so, inserting Equation 1 into Equation 7, and noting that $S_f = \sigma_f$, gives:

$$S_f^{N+1} = 2\dot{\sigma}K_c^{2-N}(N+1)/AY^2(N-2)\,(S_i^{N-2} - S_f^{N-2}) \tag{8}$$

letting

$$B \equiv 2K_c^{2-N}(N+1)/AY^2(N-2) \tag{9}$$

leads to

$$S_f^{N+1} + B\dot{\sigma}S_f^{N-2} = B\dot{\sigma}S_i^{N-2}. \tag{10}$$

Thus, if the final strength of a specimen is measured in a fracture test, the initial strength of that specimen can be computed directly from Equation 10, knowing the stressing rate, $\dot{\sigma}$. Conversely, if the initial strength of a specimen is known, the fracture strength in any constant loading-rate test can be computed from Equation 10 by numerical methods.

The logarithmic form of Equation 10 is:

$$\ln S_f = [1/(N+1)]\ln(B\dot{\sigma}) + [1/(N+1)]\ln(S_i^{N-2} - S_f^{N-2}). \tag{11}$$

Analysis of Equation 11 shows that a plot of $\ln S_f$ against $\ln \dot{\sigma}$ would have a slope of $1/(N+1)$ at low values of $\dot{\sigma}$ and a slope of zero at high values of $\dot{\sigma}$. This is consistent with the subcritical crack-growth model in which, at very high loading rates, there is not enough time for subcritical crack growth to occur and the initial and final strengths are essentially equal.

There are three methods for evaluating the constant B, based on:

(i) crack-growth measurements where N is the slope and A is the intercept of the V–K plot;

(ii) the rate-of-loading effect in which the first two terms of Equation 11 are plotted giving both the slope N and, from the intercept, B;

(iii) a logarithmic plot of the applied stress against the time to failure.

The second method was used in the present experiments and it is explained in detail in the Appendix.

This paper describes an attempt to explain the

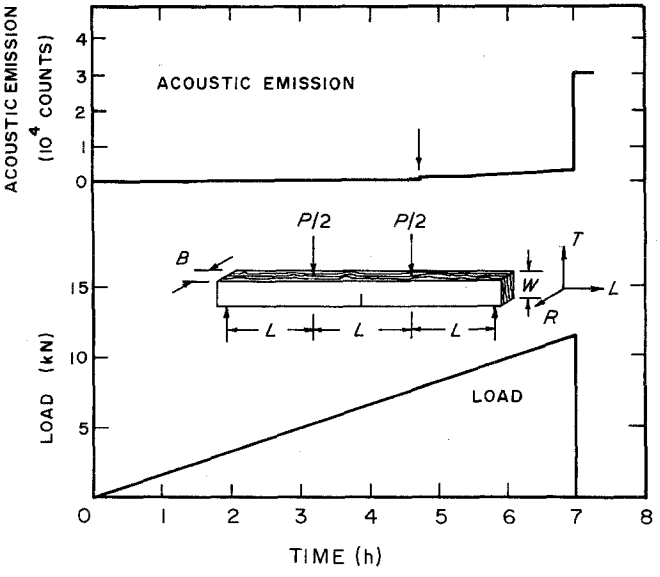

Figure 1 A typical loading curve and acoustic emission plot. The specimens were oriented so as to promote cracking in the LT system, i.e. on a plane perpendicular to the longitudinal axis and in a direction parallel to the tangential axis. In fact, cracking was a complex mixture of the LT and TL systems.

rate-of-loading effect in wood by the application of Equation 10. The ability of this fracture mechanics approach to account for existing data is tested and some new experimental results are described.

2. Experimental procedure

2.1. Material

Six hundred and forty board feet of a select commercial grade of Douglas Fir were purchased in the form of 35 mm x 216 mm x 4.88 m boards ($1\frac{3}{8}$ in. x $8\frac{1}{2}$ in. x 16 ft). The boards were carefully selected by us at the mill for straightness of grain and freedom from defects. They were then sawn and planed to produce specimens that were 35 mm x 64 mm x 914 mm ($1\frac{3}{8}$ in. x $2\frac{1}{2}$ in. x 36 in.) The finished specimens were placed in a controlled humidity room and were conditioned for 6 months at an ultimate moisture content of about 11%. Specimens were taken from the controlled humidity room at the time that they were to be tested and their moisture content was preserved by keeping them in a heavy plastic bag until they were placed in the testing machine.

2.2. The test method

The specimens were tested in four-point bending in the LT orientation [12], with the loading points 279 mm (11 in.) apart, as shown in Fig. 1. A servo-hydraulic machine was used under load control. In this method of testing, the machine attempts to increase the load on the specimen at a constant rate. As the specimen begins to fail, it becomes more compliant and the machine increases its deflection speed to maintain a constant loading rate. A typical loading curve is shown in Fig. 1. The failure stress was calculated from the highest load supported by the specimen.

Specimens were tested in the "planed" condition or in the "notched" condition. Notched specimens had a thin saw cut on the tension side midway between the central loading points as shown in Fig. 1. The stress at failure, S_f, was calculated from the simple beam formula ($S_f = 3PL/bw^2$, where P is the load, L the span, b the thickness and w the depth).

2.3. Measurement of fracture toughness

The standard equation for fracture toughness of an edge-notched beam in four-point bending is

$$K_c = \frac{6Y\sqrt{a}\,PL}{2bW^2} \qquad (12)$$

where Y is a function of the ratio of crack length, a, to beam depth, W. Equation 12 applies to materials with isotropic elastic constants and must be modified for wood. A basic equation of fracture mechanics (as applied to orthotropic material), which gives the relationship between the rate of release of stored elastic energy and the critical stress intensity factor is [10, 11]:

$$\mathscr{G}_c = (P_c^2/2b)\,(dc/da) = K_c^2/E' \qquad (13)$$

where $\mathscr{G}_c$ is the critical energy release rate, P_c is the failure load, b the specimen thickness and c the compliance. E' is the effective elastic modulus which can be computed from the relation

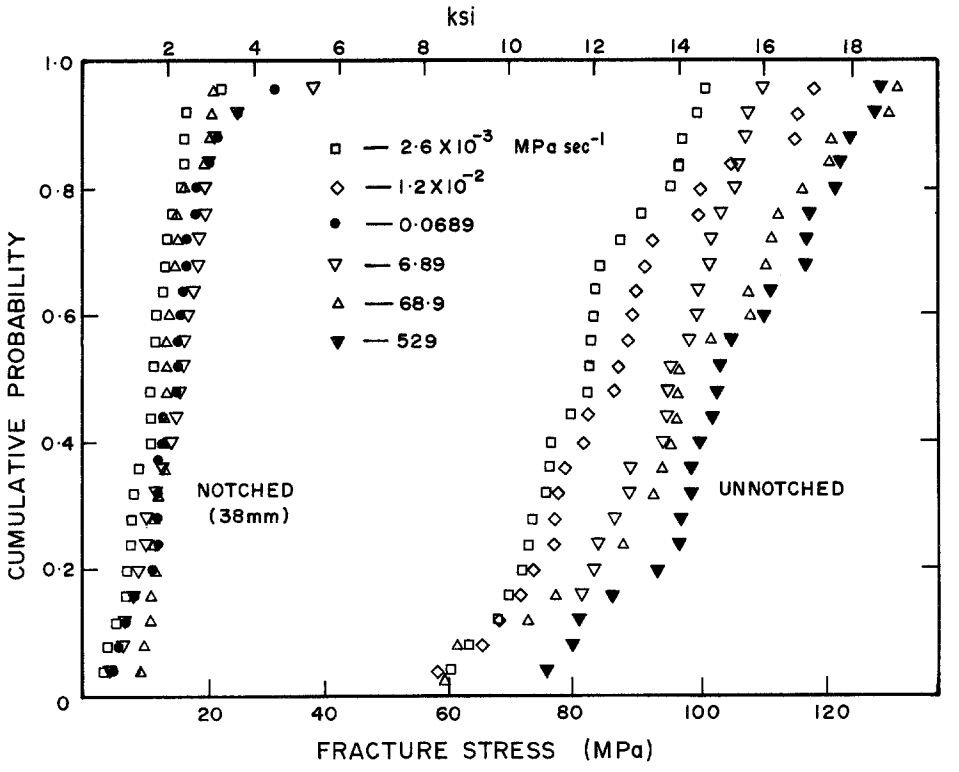

Figure 2 Plot of cumulative failure probability against strength for notched (38 mm) and unnotched specimens.

$$E' = \left\{\left(\frac{A_{11}A_{22}}{2}\right)\left[\left(\frac{A_{22}}{A_{11}}\right)^{1/2} + \frac{2A_{12} + A_{66}}{2A_{11}}\right]\right\}^{-1/2} \quad (14)$$

where A_{ij} are the anisotropic elastic compliances.

Thus, the fracture toughness of notched specimens may be determined from Equation 13 if the compliance is known as a function of crack length and if the anisotropic elastic constants are known. A compliance plot for the present tests was determined by measuring the specimen deflection at the notch position for notches of different depths. The value of the anisotropic elastic constant published by Schniewind and Pozniak [12], $E' = 1.19 \times 10^6$ psi*, was then used to obtain the fracture toughness, K_c, from Equation 13.

3. Results

3.1. Strength

Fig. 2 shows the distribution of failure strengths for notched (38 mm deep) and unnotched specimens. The notched specimens were tested at four different stressing rates ranging from 2.6×10^{-3} MPa sec^{-1} (0.38 psi sec^{-1}) to 68.9 MPa sec^{-1} (10^4 psi sec^{-1}). The unnotched specimens were tested at six different stressing rates ranging from 2.6×10^{-3} MPa sec^{-1} to 529 MPa sec^{-1}. The fastest stressing rate (529 MPa sec^{-1}) was not feasible for the notched specimens because of the large deflections involved. Apart from the expected difference in strength between the notched and unnotched specimens, Fig. 2 reveals a rate-of-loading effect only in the unnotched specimens.

The mean values of strength are plotted against stressing rate in Fig. 3. The solid lines drawn through the data were calculated from Equation 10. The value of B for this equation was obtained by a method described in detail in the Appendix. The apparent slope of the V–K plot, as obtained from the slope of the data for unnotched specimens in Fig. 3, was 59, which is experimentally indistinguishable from the earlier values (62 and 65) measured for cracks parallel to the grain [1, 2].

The broken lines in Fig. 3 are the regression lines for the 95th and 5th percentiles of Spencer's [6] dimension lumber. Thus, the mean strength of the unnotched specimens tested in the present

*10^3 psi ≡ 6.89 N m^{-2}.

TABLE I Values of K_c for Douglas Fir in the LT mode of crack propagation

Notch depth (mm)	Stressing rate (MPa sec^{-1})	K_c* (MPa m$^{1/2}$)
12.7	0.689	5.1
38	2.6×10^{-3}	3.6
38	6.89×10^{-2}	4.7
38	0.689	4.7
38	68.9	4.4
	average†	4.7

*Calculated from Equation 13 using the compliance method.
†The lowest value (at the slowest rate) was excluded from the average because of likely slow crack growth during the test.

experiments was slightly higher than the 95th percentile of Spencer's boards. When notched halfway through, the present specimens had a mean strength about the same as Spencer's 5th percentile. Furthermore, just as Spencer observed, the rate-of-loading effect was readily apparent for the stronger specimens but appeared to be absent for the weaker ones.

Fig. 4 shows the effect of notch depth on strength at a constant stressing rate (0.689 MPa sec^{-1}, 100 psi sec^{-1}). The two notch depths were 0.2 and 0.5 times the beam depth (12.7 mm and 38 mm). The specimens having a small notch had a mean strength about the same as Spencer's 50th percentile.

3.2. Fracture toughness

The values of fracture toughness obtained from the compliance-plot method are shown in Table I. Each value is the average of twenty-four tests. The low value (3.6 MPa m$^{1/2}$) obtained at a slow loading rate was not included when computing the average because it was thought that slow crack growth probably influenced the result.

It is possible to calculate the apparent flaw size in unnotched specimens by using the measured toughness and the fracture strength, according to Equation 1. The value of the constant, Y, in this equation is approximately 2.0 [13] for very small flaws. The calculated values of apparent flaw size are listed in Table II.

TABLE II Apparent flaw size* in unnotched specimens. Computed from Equation 1, with $Y = 2$ and $K_c = 4.7$ MPa m$^{1/2}$.

Stressing rate (MPa sec^{-1})	Average strength (MPa)	Apparent flaw size* (mm)
2.6×10^{-3}	79.48	1.7
1.2×10^{-2}	85.59	1.5
0.689	94.03	1.4
68.9	98.30	1.1
529	103.74	1.0

*If the flaws were notches, this would be their depth.

3.3. The morphology of fracture

The geometry assumed in the analysis of these experiments was quite simple. In the notched specimens, notches were placed in the LT orientation and loads were applied in order to promote cracking in the same orientation. Similarly, it was assumed that failure of the unnotched specimens began at small flaws on the tension side of the beam and grew in the LT orientation. The actual experience, however, was much more complex.

Often there were numerous cracks that grew parallel to the axis of the beam, i.e. in the TL orientation [12]. These cracks would link up at random across the grain so that the crack followed a very tortuous path. Thus, much of the subcritical crack growth was parallel rather than perpendicular to the grain.

Careful observations of the initiation of fracture, revealed that fracture always started on the tension side of the beam. After considerable cracking parallel and perpendicular to the grain, the compliance was so reduced, that buckling occurred under the inner loading points. Buckling further reduced the compliance so that the machine was no longer able to increase the load and failure by stiffness collapse followed. Thus, even the definition of failure is difficult in the case of wood. The initiation of failure as shown by the acoustic emission data in Fig. 1 occurs at a much lower load than ultimate collapse. For design purposes it is likely that crack initiation is a safer failure criterion than collapse, but in the present experiments, collapse was more easily measured.

The details of the fracture process are relevant to the validity of the fracture-mechanics analysis used in the present paper. However, they are so complex that considerable work remains to be completed. Each fractured beam has been photographed and the relation between strength and fracture morphology is being examined. These results will be described in a subsequent paper.

4. Discussion

This paper describes an attempt to understand the

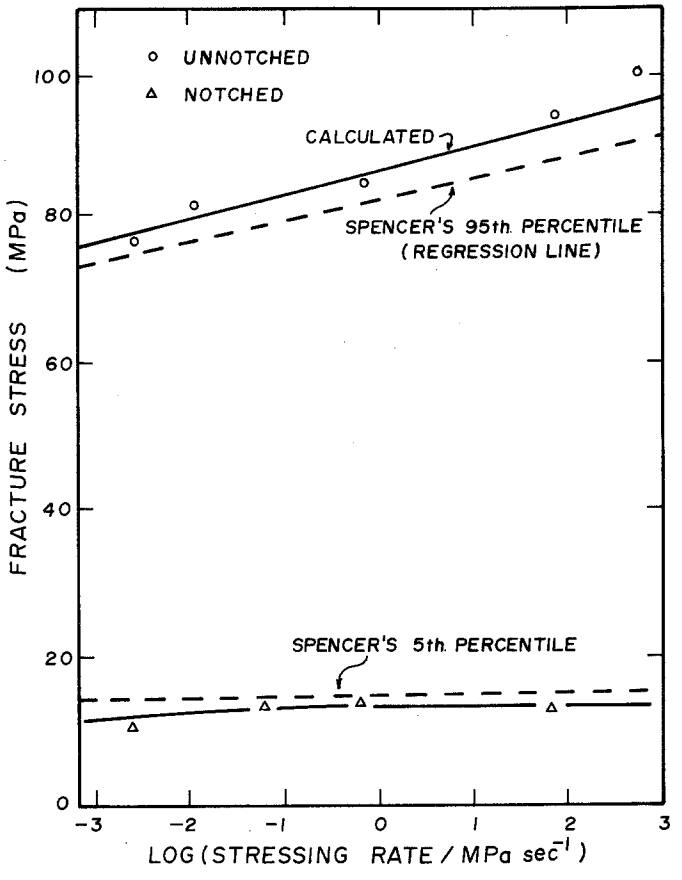

Figure 3 The rate-of-loading effect for notched (38 mm) and unnotched specimens. Each point is the average of 24 tests. The solid line was calculated from Equation 10 by the method described in the Appendix. The broken lines are from Spencer's results on dimension lumber [6].

kinetics of wood fracture. The approach was to measure the rate-of-loading effect in notched and unnotched specimens and to see whether the results could be adequately explained by a fracture mechanics model. Clearly, there are some difficulties in applying the simple model, assuming opening-mode fracture, to the complex, possibly mixed-mode fracture of wood. Nevertheless, the agreement between theory and experiment, shown by Fig. 3, is very encouraging. It is, of course, no

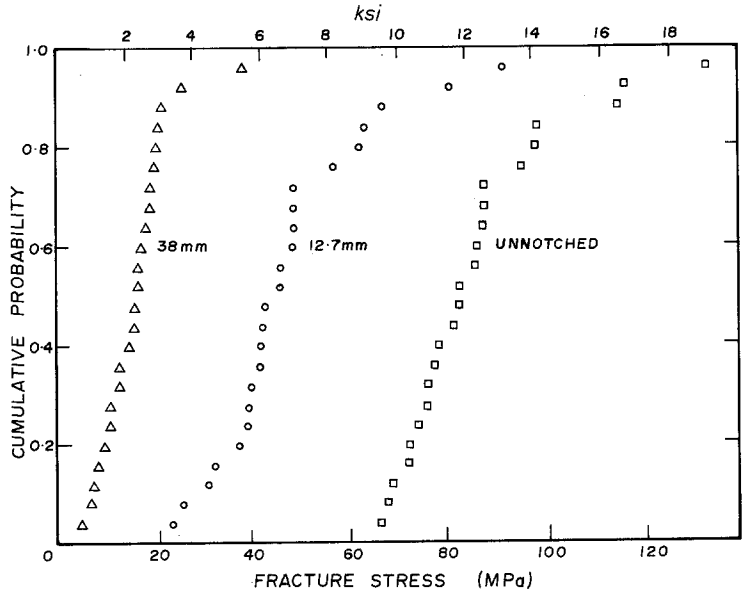

Figure 4 Effect of notch depth at the same stressing rate (0.689 MPa sec^{-1}, 100 psi sec^{-1}).

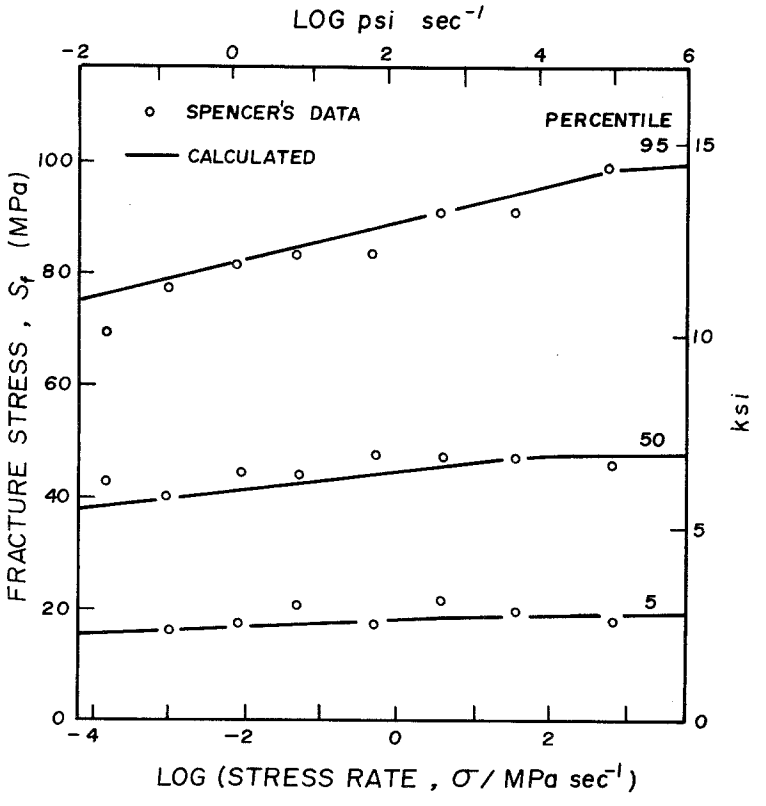

Figure 5 Spencer's data points for the 95th, 50th and 5th percentiles of strength of dimension lumber. The lines are calculated from the fracture-mechanics model by the method described in the Appendix.

surprise that the calculated curve fits the data for unnotched specimens so well, since the slope and position of the line are obtained from those data. However, having extracted the fracture-mechanics parameters N and B from the data for strong specimens, the theory correctly predicts the behaviour of notched specimens (Fig. 3) and dimension lumber as shown in Fig. 5. Thus, the present work confirms Spencer's result [6] by showing that weak specimens appear to have an attenuated rate-of-loading effect and it further shows that the fracture mechanics theory predicts the observed effect. Furthermore, the theory provides the following relatively simple explanation: There are two regions of stressing-rate behaviour, the high-rate region where strength is independent of rate, and the low-rate region where strength is influenced by subcritical crack growth. The boundary between these two regions shifts to lower stressing rates as the initial strength decreases, as shown in Fig. 6. The physical reason for this shift in the boundary is simply that weaker specimens, having larger cracks, are less influenced by a small amount of subcritical crack growth. This is illustrated quite clearly by the data in Table II. If the flaw size at the highest loading rate is taken as the initial flaw size (1.0 mm), then subcritical growth of 0.7 mm is sufficient to reduce the strength to the value measured at the slowest loading rate. The same amount of subcritical growth in a specimen already having a notch or flaw 38 mm deep would have very little effect on the strength.

The second factor giving the appearance of an attenuated rate-of-loading effect for weak specimens is just the logarithmic relation between fracture strength and stressing rate as expressed by Equation 11. When the strength is plotted linearly as in Figs 3, 5 and 6, the slope decreases as the initial strength decreases. When plotted on logarithmic axes, the same data can be equally well represented by a set of parallel lines having a slope of $1/(N+1)$. Thus, the difference between the initial strength and the strength at a very slow loading rate, 6.89×10^{-5} MPa sec^{-1} (0.01 psi sec^{-1}), is only 3.4 MPa (495 psi) for the 5th percentile of specimens, while it is 23.1 MPa (3357 psi) for the 95th percentile. The experimental precision is the same for both samples and it is therefore much easier to detect the difference for the strong specimens. This is not to say that the calculated difference is proportionately the same for weak and strong specimens. It is 18% for the weak ones and about 24% for the strong ones.

According to the fracture-mechanics theory,

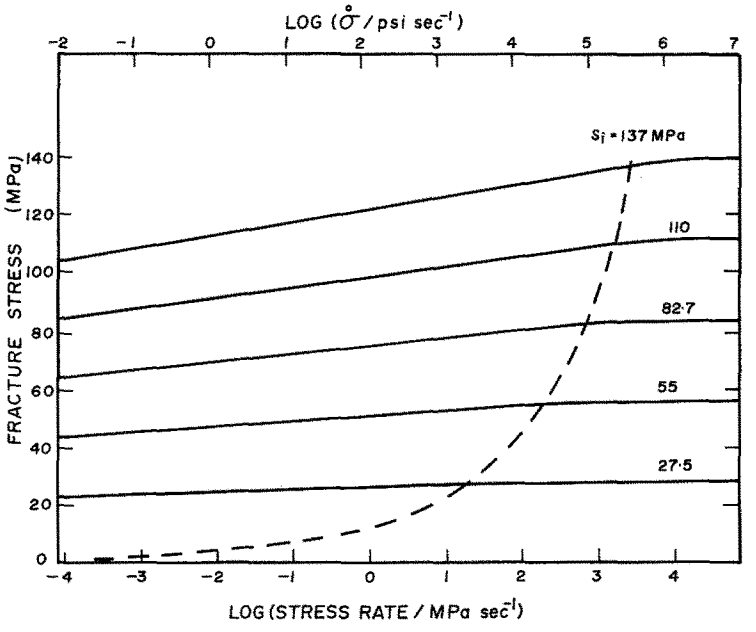

Figure 6 Calculated examples of the rate-of-loading effect for Douglas Fir as a function of the initial strength. The broken line is the calculated position of the boundary between the stress-rate insensitive region (high stressing rates) and the sub-critical crack-growth region as described by Equation A6.

the duration of load-effect is another manifestation of subcritical crack growth. This effect is observed when a constant stress is applied to the specimens and the time to failure is measured. If Equation 4 is integrated at constant stress, we obtain the result:

$$t_f = B\sigma_a^{-2}\left[(\sigma_a/S_i)^{2-N} - 1\right] \qquad (15)$$

where t_f is the time to failure. Equation 15 is plotted in Fig. 7, showing that, like the rate-of-loading effect, the duration-of-load effect appears to diminish as the initial strength decreases. On a logarithmic plot, the lines shown in Fig. 7 would be straight and parallel with a slope of approximately $-1/N$.

The "Adjustment of Working Stresses for Various Durations of Load" as published by the US Forest Products Laboratory [5] is also shown in Fig. 7. It has a significantly steeper slope than the results obtained from the present experiments, but for weak specimens the reduction in strength for a 50-year life is virtually the same. Since it is

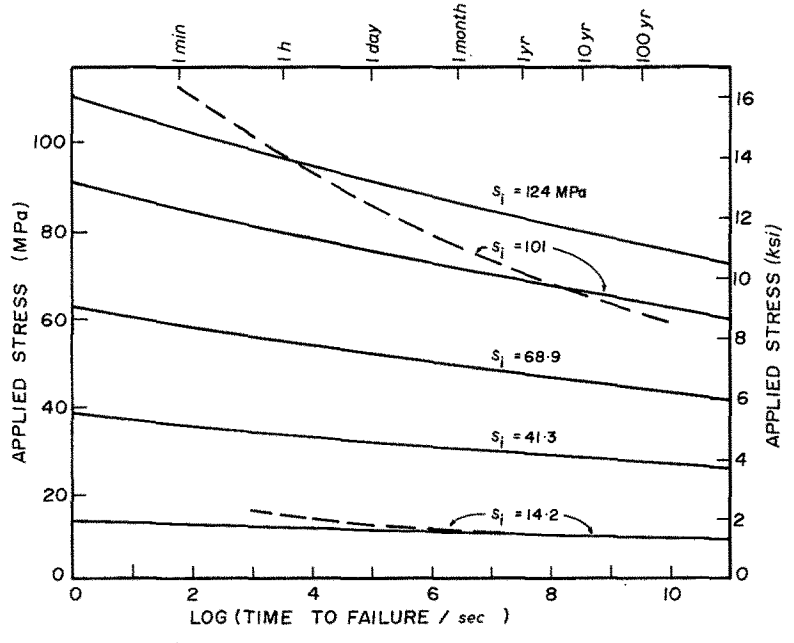

Figure 7 The duration-of-load effect as a function of initial strength, calculated from Equation 15. Two examples of the "Adjustment of Working Stresses for Various Durations of Load", US Forest Products Laboratory, are shown in broken lines.

the usual practice to assign working stresses on the basis of the strength at the 5th percentile, there would appear to be no serious conflict between the present results and the normal design procedure. Thus, these results appear to support both the practice of adjusting for the duration-of-load effect and the approximate magnitude of the adjustment. However, the curves of Fig. 7 were computed from average values of the parameters N and $B = f(K_c)$. The uncertainty in these parameters is quite large as can be judged from the dispersion of the data in Fig. 2. The resulting uncertainty in predicting the time to failure has been shown to render plots such as Fig. 7 relatively useless. Fortunately, two recent papers [14, 15] have described statistical methods for reducing the uncertainty in failure prediction. The methods are based on the same fracture-mechanics principles described in this paper and should be readily applicable to wood.

Acknowledgements

This paper was written while one of the authors (J. S. Nadeau) was a guest worker at the US National Bureau of Standards. He is grateful for the interest and assistance that he received there. The work was supported by a Grant from the Science Council of British Columbia.

Appendix: Method of calculating the fracture strength S_f, knowing the initial strength S_i, and the stressing rate $\dot{\sigma}$

The constant B in Equation 10 can be evaluated from a logarithmic plot of S_f against $\dot{\sigma}$ as shown in Fig. 8. If all of the data appear to lie on a straight line, as in the present case, it is assumed that σ_c lies above the stressing rate range of the tests. B is then obtained from the relation

$$\log B = (N+1)\log S_{f_0} - (N-2)\log S_i. \quad \text{(A1)}$$

In the present experiments the value obtained was $B = 1.692 \times 10^7$.

Knowing B, it was then possible to solve Equation 10 for a given initial strength and $\dot{\sigma}$. This was done by rearranging the equation into the following form:

$$X^{N+1} + \beta X^{N-2} - 1 = 0 \quad \text{(A2)}$$

where

$$X = (S_f/bS_i)^{N+1} \quad \text{(A3)}$$

$$b = [B\dot{\sigma}/S_i^3]^{1/(N+1)} \quad \text{(A4)}$$

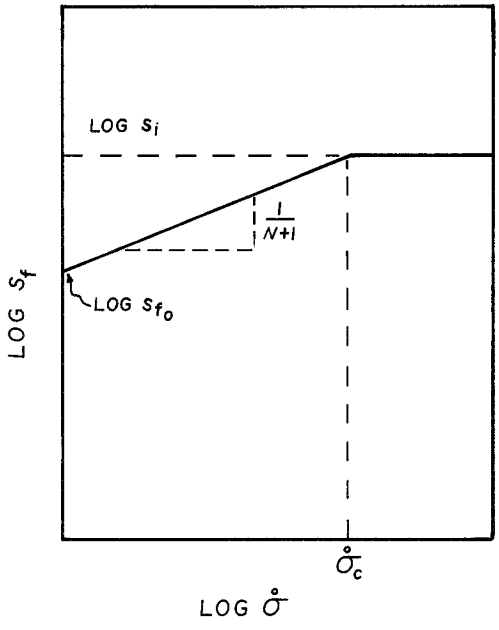

Figure 8 Method of calculating N and B from stressing-rate data.

$$\beta = b^{N-2}. \quad \text{(A5)}$$

Equation A2 was then solved by an algorithm employing Newton's method of roots.

The value of $\dot{\sigma}_c$ can, in principle be obtained by drawing tangents to the two limbs of the stressing rate curve as shown in Fig. 8. A more accurate way is to differentiate Equation 10 with respect to $\dot{\sigma}$ and to solve the resulting differential equation at $S_f = S_i$. The expression for the critical stressing rate is then:

$$\dot{\sigma}_c = S_i^3/B. \quad \text{(A6)}$$

This function is plotted in Fig. 6.

References

1. S. MINDESS, J. S. NADEAU and J. D. BARRETT, *Wood Sci.* 8 (1) (1975) 389.
2. *Idem, ibid.* 8 (4) (1976) 262.
3. C. C. GERHARDS, "Effect of Duration and Rate of Loading on Strength of Wood and Wood-based Materials", United States Forest Products Laboratory, Madison, Wisconsin, Research Paper no. 283.
4. J. D. BARRETT and R. O. FOSCHI, *Canad. J. Civil. Eng.* 5 (1973) 505.
5. Wood Structural Design Data, 1978 edn., National Forest Products Association, 1619 Massachusetts Ave., N.W., Washington, D.C. 13.
6. R. SPENCER, "Rate of Loading Effect in Bending for Douglas-Fir Lumber", 1st International Conference on Wood Fracture, Banff, Alberta, Canada, August (1978).
7. A. G. EVANS, *Int. J. Fract.* **10** (1974) 251.

8. J. E. RITTER JR and C. L. SHERBURNE, *J. Amer. Ceram. Soc.* **54** (1971) 601.
9. J. E. RITTER JR, in "Fracture Mechanics of Ceramics", Vol. 4, edited by R. C. Bradt, D. P. H. Hasselman and F. F. Lange, (Plenum Press, New York, 1978) p. 667.
10. P. W. R. BEAUMONT and A. S. TETLEMAN, The Fracture Strength and Toughness of Composite Materials, in "Failure Modes in Composites", edited by Istvan Toth, (AIME, 1972) p. 49.
11. G. C. SIH, P. C. PARIS and G. R. IRWIN, *Int. J. Fract. Mech.* 1 (1965) 189.
12. A. P. SCHNIEWIND and R. A. POZNIAK, *Eng. Fract. Mech.* **2** (1971) 223.
13. W. F. BROWN JR and J. E. SRAWLEY, *ASTM STP* **410** (1966) 13.
14. J. E. RITTER JR, N. BANDYOPADHYAY and K. JAKUS, *J. Amer. Ceram. Soc.* **62** (1979) 542.
15. S. M. WIEDERHORN, to be published.

Received 30 November 1981
and accepted 12 February 1982